

LA-UR-05-3781

Approved for public release;
distribution is unlimited.

Title: Discrete Diffusion Monte Carlo for grey Implicit Monte Carlo simulations

Author(s): Jeffery D. Densmore
Todd J. Urbatsch
Thomas M. Evans
Michael W. Buksas

Submitted to: American Nuclear Society Topical Meeting in Mathematics & Computations, Avignon, France, 2005



Los Alamos National Laboratory, an affirmative action/equal opportunity employer, is operated by the University of California for the U.S. Department of Energy under contract W-7405-ENG-36. By acceptance of this article, the publisher recognizes that the U.S. Government retains a nonexclusive, royalty-free license to publish or reproduce the published form of this contribution, or to allow others to do so, for U.S. Government purposes. Los Alamos National Laboratory requests that the publisher identify this article as work performed under the auspices of the U.S. Department of Energy. Los Alamos National Laboratory strongly supports academic freedom and a researcher's right to publish; as an institution, however, the Laboratory does not endorse the viewpoint of a publication or guarantee its technical correctness.

DISCRETE DIFFUSION MONTE CARLO FOR GREY IMPLICIT MONTE CARLO SIMULATIONS

Jeffery D. Densmore, Todd J. Urbatsch, Thomas M. Evans, and Michael W. Buksas

Transport Methods Group (CCS-4), Los Alamos National Laboratory
PO Box 1663, MS D409, Los Alamos, New Mexico 87545
jdd@lanl.gov; tmonster@lanl.gov; tme@lanl.gov; mwbuksas@lanl.gov

ABSTRACT

Discrete Diffusion Monte Carlo (DDMC) is a hybrid transport-diffusion method for Monte Carlo simulations in diffusive media. In DDMC, particles take discrete steps between spatial cells according to a discretized diffusion equation. Thus, DDMC produces accurate solutions while increasing the efficiency of the Monte Carlo calculation. In this paper, we extend previously developed DDMC techniques in several ways that improve the accuracy and utility of DDMC for grey Implicit Monte Carlo calculations. First, we employ a diffusion equation that is discretized in space but is continuous time. Not only is this methodology theoretically more accurate than temporally discretized DDMC techniques, but it also has the benefit that a particle's time is always known. Thus, there is no ambiguity regarding what time to assign a particle that leaves an optically thick region (where DDMC is used) and begins transporting by standard Monte Carlo in an optically thin region. In addition, we treat particles incident on an optically thick region using the asymptotic diffusion-limit boundary condition. This interface technique can produce accurate solutions even if the incident particles are distributed anisotropically in angle. Finally, we develop a method for estimating radiation momentum deposition during the DDMC simulation. With a set of numerical examples, we demonstrate the accuracy and efficiency of our improved DDMC method.

KEYWORDS: radiative transfer, Monte Carlo, hybrid transport-diffusion

1. INTRODUCTION

The Implicit Monte Carlo (IMC) method [1] has been shown to be an effective technique for solving radiative transfer problems via Monte Carlo simulation. In IMC, the absorption and emission of radiation by the material within a time step is approximated semi-implicitly by an effective scatter process. This effective scattering helps stabilize the calculation and allows larger time steps to be used than in a purely explicit method [2, 3] (where radiation absorbed in a given time step cannot be re-emitted until the following time step). However, in optically thick regions not only is the mean-free path of a particle small, but also the collisions are dominated by effective scatters. Thus, the transport process can be characterized as *diffusive*, the particle histories are extremely long, and the Monte Carlo simulation becomes computationally inefficient.

Due to the diffusive nature of such problems, one would like to employ a hybrid method that uses standard transport theory in optically thin regions and the diffusion approximation in optically

thick regions. Ideally, this hybrid technique would produce accurate solutions while being more efficient than a pure Monte Carlo calculation. One such hybrid transport-diffusion method is the Random Walk (RW) technique [4, 5]. In RW, several Monte Carlo transport steps are replaced by a macrostep over a spherical subregion of the cell centered about the particle's current position, thus increasing the overall efficiency of the simulation. Each RW step is governed by an analytic diffusion solution within the sphere, and the minimum allowable sphere radius is limited to ensure the accuracy of the diffusion solution. As a particle nears a cell boundary, the radius of the sphere is reduced, RW is disabled, and the particle is transported by standard Monte Carlo. Thus, the efficiency gain when employing RW decreases with increasing spatial resolution.

A new hybrid transport-diffusion method that is currently under development is Discrete Diffusion Monte Carlo (DDMC) [6–8]. In DDMC, particles take discrete steps between spatial cells according to a discretized diffusion equation, with each discrete step replacing many small transport steps. Since a particle can travel to a new cell each DDMC step, as opposed to across a spatial subdomain within a cell, DDMC should be able to provide a greater efficiency gain over standard Monte Carlo than RW.

Urbatsch, Morel, and Gulick [6] have developed a DDMC method for steady-state neutron transport problems, while the DDMC technique of Evans, Urbatsch, and Lichtenstein [7] is designed to work with the equilibrium diffusion equation [9]. Gentile [8] has successfully applied DDMC (which he refers to as Implicit Monte Carlo Diffusion) to IMC simulations. In this paper, we extend these previously developed DDMC methods in several ways that improve the accuracy and utility of DDMC for grey (i.e. frequency-independent) IMC calculations.

First, we employ a diffusion equation that is discretized in space, but is continuous in time. In addition to being theoretically more accurate than temporally discretized DDMC implementations [7, 8], our methodology always retains the time of a particle. Thus, there is no ambiguity regarding what time to assign a “DDMC particle” (i.e. a particle transporting in an optically thick region according to DDMC) that leaves an optically thick region and is converted into a “Monte Carlo particle” (i.e. a particle transporting in an optically thin region according to standard Monte Carlo).

Second, we use an improved interface method for converting Monte Carlo particles incident on an optically thick region into DDMC particles [10]. This technique, which is based on the asymptotic diffusion-limit boundary condition [11], produces accurate solutions in the interior of optically thick regions regardless of the angular distribution of the incident Monte Carlo particles. Previous DDMC implementations that employ the Marshak boundary condition [6, 7, 12] can behave poorly if the incident Monte Carlo particles are strongly anisotropic [10].

Finally, we develop a method for calculating radiation momentum deposition during the DDMC simulation. In coupled radiation-hydrodynamics problems, the calculation of fluid motion requires estimates of both the energy and momentum deposited in the material by the radiation [13, 14]. The estimation of energy deposition is straightforward in both Monte Carlo and DDMC simulations; when a particle is absorbed its energy is allocated to the material. However, the calculation of momentum deposition in DDMC is difficult since momentum is a direction-dependent quantity, and DDMC particles have no angular information. To avoid this

difficulty, our momentum deposition estimator is based on the rate at which DDMC particles cross cell surfaces. Thus, angular information is extracted from the direction a particle travels to a new cell.

In the remainder of this paper we briefly overview the analytic equations governing grey thermal radiative transfer, the corresponding IMC method, and difficulties with IMC when the opacity is large. We then develop our improved DDMC method, and show how it can be combined with standard Monte Carlo in an IMC simulation. Next, with a set of numerical examples, we demonstrate both the accuracy and improved efficiency over standard Monte Carlo of our new DDMC method. We conclude with a brief discussion.

2. BACKGROUND

In the absence of internal sources and scattering, the planar-geometry, grey radiative transfer equations are [13–15]

$$\frac{1}{c} \frac{\partial I}{\partial t} + \mu \frac{\partial I}{\partial x} + \sigma I = \frac{1}{2} \sigma a c T^4, \quad (1)$$

and

$$C_v \frac{\partial T}{\partial t} = \int_{-1}^1 \sigma \left(I - \frac{1}{2} a c T^4 \right) d\mu. \quad (2)$$

Here, $0 < x < X$ is the spatial variable, $-1 \leq \mu \leq 1$ is the angular variable, $t > 0$ is the temporal variable, $I(x, \mu, t)$ is the radiation intensity, $T(x, t)$ is the material temperature, $\sigma(x, T)$ is the opacity, $C_v(x, T)$ is the heat capacity, a is the radiation constant, and c is the speed of light. To complete the problem description, appropriate initial conditions apply to I and T at $t = 0$, and to I for incoming directions at the left ($x = 0$) and right ($x = X$) boundaries.

In order to solve Eqs. 1 and 2 using IMC, we first prescribe a temporal grid $0 = t_0 < t_1 < t_2 < \dots$. Then, within each time step $t_n < t < t_{n+1}$, the emission source on the right side of Eq. 1 is semi-implicitly approximated using Eq. 2. The resulting equations governing the IMC method are [1]

$$\frac{1}{c} \frac{\partial I}{\partial t} + \mu \frac{\partial I}{\partial x} + \sigma_n I = \frac{1}{2} (1 - f_n) \sigma_n \int_{-1}^1 I(x, \mu', t) d\mu' + \frac{1}{2} f_n \sigma_n a c T_n^4, \quad (3)$$

and

$$C_v \frac{\partial T}{\partial t} = \int_{-1}^1 f_n \sigma_n \left(I - \frac{1}{2} a c T_n^4 \right) d\mu, \quad (4)$$

where the subscript n refers to a material property evaluated at the beginning of the time-step temperature. In addition, the *Fleck factor* f_n is given by

$$f_n = \frac{1}{1 + \beta_n \sigma_n c \Delta t_n}, \quad (5)$$

where

$$\beta_n = \frac{4aT_n^3}{C_{v,n}}, \quad (6)$$

and $\Delta t_n = t_{n+1} - t_n$ is the size of the time step.

Within each time step, Eq. 3 can be solved for I using standard Monte Carlo simulation. The initial conditions are given by the prescribed initial radiation intensity and material temperature for the first time step, or by the results of the previous time step for subsequent time steps. Note that we have divided the physical opacity σ_n into an isotropic effective-scattering opacity $(1 - f_n)\sigma_n$ and a corresponding effective-absorption opacity $f_n\sigma_n$. Thus, the IMC method approximates the absorption and emission of radiation within a time step by isotropic scattering. Accordingly, the emission source has been reduced by a factor f_n . After I has been determined, the material temperature is updated using the radiation absorbed and emitted over the time step to evaluate Eq. 4.

In addition to the net radiation energy deposited in the material, coupled radiation-hydrodynamics calculations also require an estimate of the radiation momentum deposited in the material. The specific momentum deposition (the momentum deposited per unit volume per unit time) corresponding to Eq. 1 is given by [13, 14]

$$p(x, t) = \frac{\sigma}{c} \int_{-1}^1 \mu I(x, \mu, t) d\mu . \quad (7)$$

Integrals of this form can be estimated by Monte Carlo simulation in a straightforward manner. In this paper, we employ a track-length estimator [16], and approximate the opacity by its explicit value σ_n .

Eqs. 3 and 4 provide a systematic method for solving Eqs. 1 and 2 via Monte Carlo. However, in materials where the opacity is large, the Monte Carlo simulation can become inefficient. Not only is the mean-free path between collisions small, but also, from Eq. 5, the Fleck factor is small and the collisions are primarily scattering events. Thus, the problem is highly diffusive and the Monte Carlo histories are extremely long. In the next section we develop a hybrid transport-diffusion technique for solving Eq. 3 that is much more efficient than standard Monte Carlo when the opacity is large, and still yields accurate results.

3. DISCRETE DIFFUSION MONTE CARLO

We now develop the equations governing our improved DDMC method. This technique is based on a diffusion approximation to Eq. 3, so it should yield accurate solutions when used in appropriate regions (i.e. when σ_n is large and f_n is small). In addition, we will show later that the DDMC transport process consists of discrete steps between spatial cells. Thus, DDMC should be more computationally efficient than a standard Monte Carlo simulation of Eq. 3.

We begin by considering a subregion $X_L < x < X_R$ of the problem domain that has been designated for simulation by DDMC. In this region we develop a cell-centered discretization of the diffusion equation corresponding to Eq. 3. This derivation is similar to the work of Szilard and Pomraning [17], except that we only discretized the spatial variable and treat time continuously. Integrating Eq. 3 over all directions, we have

$$\frac{1}{c} \frac{\partial \phi}{\partial t} + \frac{\partial F}{\partial x} + f_n \sigma_n \phi = f_n \sigma_n a c T_n^4 , \quad (8)$$

where the scalar intensity is

$$\phi(x, t) = \int_{-1}^1 I(x, \mu, t) d\mu \quad , \quad (9)$$

and the radiative flux is given by

$$F(x, t) = \int_{-1}^1 \mu I(x, \mu, t) d\mu \quad . \quad (10)$$

Next, we divide the DDMC region into a spatial grid $X_L = x_{1/2} < x_{3/2} < \dots < x_{J+1/2} = X_R$ consisting of J cells. Integrating Eq. 8 over spatial cell j yields

$$\frac{1}{c} \frac{d}{dt} \phi_j + \frac{1}{\Delta x_j} (F_{j+1/2} - F_{j-1/2}) + f_{n,j} \sigma_{n,j} \phi_j = f_{n,j} \sigma_{n,j} a c T_{n,j}^4 \quad . \quad (11)$$

In Eq. 11, the cell-averaged scalar intensity is given by

$$\phi_j(t) = \frac{1}{\Delta x_j} \int_{x_{j-1/2}}^{x_{j+1/2}} \phi(x, t) dx \quad , \quad (12)$$

the cell-edge flux is

$$F_{j+1/2}(t) = F(x_{j+1/2}, t) \quad , \quad (13)$$

$\Delta x_j = x_{j+1/2} - x_{j-1/2}$ is the cell width, and we have used appropriate cell-averaged quantities for the material properties.

3.1. Interior Cells

We continue our derivation of a cell-centered discretized diffusion equation for cells $2 \leq j \leq J - 1$ in the interior of the DDMC region. We approximate the cell-edge flux using Fick's law [12, 17],

$$F_{j+1/2} = - \frac{1}{3\sigma_n} \frac{\partial \phi}{\partial x} \Big|_{x=x_{j+1/2}} \quad . \quad (14)$$

Employing a finite-difference approximation to Eq. 14, we can express $F_{j+1/2}$ in cell j as

$$F_{j+1/2} = - \frac{2}{3\sigma_{n,j+1/2}^- \Delta x_j} (\phi_{j+1/2} - \phi_j) \quad , \quad (15)$$

or in cell $j + 1$ as

$$F_{j+1/2} = - \frac{2}{3\sigma_{n,j+1/2}^+ \Delta x_{j+1}} (\phi_{j+1} - \phi_{j+1/2}) \quad . \quad (16)$$

In Eqs. 15 and 16, $\phi_{j+1/2}$ is an appropriately defined cell-edge scalar intensity. In addition, we have used a face-averaged approximation for the opacity in each cell. We will discuss the evaluation of these opacities later in this paper.

Next, equating Eqs. 15 and 16 and solving for the cell-edge scalar intensity, we have

$$\phi_{j+1/2} = \frac{1}{\sigma_{n,j+1/2}^- \Delta x_j + \sigma_{n,j+1/2}^+ \Delta x_{j+1}} \left(\sigma_{n,j+1/2}^+ \Delta x_{j+1} \phi_j + \sigma_{n,j+1/2}^- \Delta x_j \phi_{j+1} \right) . \quad (17)$$

Then, using Eq. 17 to evaluate Eq. 15 or 16, an approximate expression for the cell-edge flux is

$$F_{j+1/2} = -\frac{2}{3} \frac{1}{\sigma_{n,j+1/2}^- \Delta x_j + \sigma_{n,j+1/2}^+ \Delta x_{j+1}} (\phi_{j+1} - \phi_j) . \quad (18)$$

Substituting Eq. 18 and a similar expression for $F_{j-1/2}$ into Eq. 11, the DDMC equation for cells $2 \leq j \leq j-1$ is

$$\begin{aligned} \frac{1}{c} \frac{d}{dt} \phi_j + (\sigma_{L,j} + \sigma_{R,j} + f_{n,j} \sigma_{n,j}) \phi_j \\ = f_{n,j} \sigma_{n,j} a c T_{n,j}^4 + \frac{1}{\Delta x_j} (\sigma_{L,j+1} \phi_{j+1} \Delta x_{j+1} + \sigma_{R,j-1} \phi_{j-1} \Delta x_{j-1}) . \end{aligned} \quad (19)$$

In Eq. 19, we have defined the left-leakage opacity as

$$\sigma_{L,j} = \frac{2}{3 \Delta x_j} \frac{1}{\sigma_{n,j-1/2}^+ \Delta x_j + \sigma_{n,j-1/2}^- \Delta x_{j-1}} , \quad (20)$$

and the right-leakage opacity as

$$\sigma_{R,j} = \frac{2}{3 \Delta x_j} \frac{1}{\sigma_{n,j+1/2}^- \Delta x_j + \sigma_{n,j+1/2}^+ \Delta x_{j+1}} . \quad (21)$$

We now give Eq. 19 a Monte Carlo interpretation. This equation can be viewed as a time-dependent infinite medium transport problem for each cell. Thus, DDMC particles have no position or angular information, but their current cell and time are always known. DDMC particles stream in time (but not in space) at the speed of light until experiencing a collision. The time to collision τ can be sampled similarly to the usual method of sampling distance to collision [16],

$$\tau = -\frac{1}{c} \frac{1}{\sigma_{L,j} + \sigma_{R,j} + f_{n,j} \sigma_{n,j}} \ln \xi , \quad (22)$$

where ξ is a random number uniformly distributed between 0 and 1.

If the time to collision is less than the time remaining in the time step, the DDMC particle experiences an appropriately sampled collision type. From the second term on the left side of Eq. 19, a collision can be an absorption reaction, a left-leakage reaction, or a right-leakage reaction. If the collision is an absorption reaction, the particle history is terminated, as in standard Monte Carlo. If the DDMC particle undergoes a leakage reaction, it is transferred to the appropriate neighboring cell and the simulation continues.

If the time to collision is greater than the time remaining in the time step, the DDMC particle reaches the end of the time step and is stored for simulation in the next time step. Since in the next time step DDMC may not be used in the current cell, the DDMC particle is placed uniformly and isotropically within the cell.

The right side of Eq. 19 contains not only the usual emission source term, but also source terms corresponding to DDMC particles undergoing leakage reactions in neighboring cells and being transferred to the current cell. These leakage source terms can be interpreted as the total rate at which particles experience appropriate leakage reactions in adjacent cells (i.e. the rate per volume times the volume of the cell) divided by the volume of the current cell, such that these leaked particles are distributed evenly over the cell.

It is interesting to note that as the opacity increases, not only do the leakage opacities decrease (from Eqs. 20 and 21), but also the absorption opacity $f_n\sigma_n$ is $O(1)$ (from Eq. 5). Thus, from Eq. 22, the time between collisions is not excessively small, the collisions are primarily absorptions, and DDMC particle histories are relatively short. This is exactly the opposite effect that a large opacity has on a standard Monte Carlo simulation of Eq. 3.

We now discuss the evaluation of the opacities in Eqs. 20 and 21. According to Szilard and Pomraning, if one of the opacities is very large, then the entire expression can be small and radiation will not propagate [17]. This lack of propagation is commonly seen when the opacity is strongly temperature dependent and the material is cold. To prevent this unphysical behavior, Szilard and Pomraning suggest evaluating the opacities at a common cell-edge temperature. For example, in Eq. 21 we calculate $\sigma_{n,j+1/2}^-$ using the material properties in cell j , and $\sigma_{n,j+1/2}^+$ using the material properties in cell $j+1$. However, both opacities are evaluated at the following cell-edge temperature [17]:

$$T_{n,j+1/2} = \left(\frac{T_{n,j}^4 + T_{n,j+1}^4}{2} \right)^{1/4} . \quad (23)$$

A similar technique can be used to calculate Eq. 20.

3.2. Interface Cells

Next, we develop a technique for interfacing DDMC with standard Monte Carlo by deriving a cell-centered equation for cell 1 on the left boundary of the DDMC region. A similar analysis can be performed for cell J . Writing Eq. 11 for $j=1$, and using Eq. 18 for $F_{3/2}$, we have

$$\frac{1}{c} \frac{d}{dt} \phi_1 + (\sigma_{R,1} + f_{n,1}\sigma_{n,1}) \phi_{n,1} - \frac{1}{\Delta x_1} F_{1/2} = f_{n,1}\sigma_{n,1} ac T_{n,1}^4 + \frac{1}{\Delta x_1} \sigma_{L,2} \phi_2 \Delta x_2 , \quad (24)$$

where we have made use of Eqs. 20 and 21. To complete this derivation, we must find an approximate expression for the flux at the boundary of the DDMC region.

Instead of using the usual Marshak boundary condition [12, 17], we consider the asymptotic

diffusion-limit boundary condition [11],

$$2 \int_0^1 W(\mu) I_b(X_L, \mu, t) d\mu = \phi(X_L, t) - \frac{\lambda}{\sigma_n} \frac{\partial \phi}{\partial x} \Big|_{x=X_L} . \quad (25)$$

In Eq. 25, I_b is the radiation intensity incident on the boundary of the DDMC region due to Monte Carlo particles, while $\lambda \approx 0.7104$ is the *extrapolation distance*. In addition, $W(\mu)$ is a transcendental function well approximated by

$$W(\mu) \approx \mu + \frac{3}{2} \mu^2 . \quad (26)$$

Eq. 25 can be derived in an asymptotic analysis of Eq. 3 as σ_n becomes large and f_n becomes small. This is exactly the situation in which DDMC is employed. In addition, the incident intensity is weighted by $W(\mu)$, which takes into account the angular distribution of the Monte Carlo particles. An interface method based on Eq. 25 will be able to produce accurate results in the interior of the DDMC region even if the incident intensity is anisotropic [10]. In contrast, the Marshak boundary condition treats all angular distributions identically, and can produce inaccurate solutions for strongly anisotropic incident particles [10].

To express $F_{1/2}$ using Eq. 25, we approximate the derivative on the right side with a finite difference. We then have

$$2 \int_0^1 W(\mu) I_b(X_L, \mu, t) d\mu = \phi_{1/2} - \frac{\lambda}{2\sigma_{n,1}\Delta x_1} (\phi_1 - \phi_{1/2}) , \quad (27)$$

where $\sigma_{n,1}$ is the cell-averaged opacity in cell 1, and $\phi_{1/2}$ is an appropriately defined cell-edge scalar intensity. Solving Eq. 27 for $\phi_{1/2}$ yields

$$\phi_{1/2} = \frac{2\lambda}{\sigma_{n,1}\Delta x_1 + 2\lambda} + \frac{2\sigma_{n,1}\Delta x_1}{\sigma_{n,1}\Delta x_1 + 2\lambda} \int_0^1 W(\mu) I_b(X_L, \mu, t) d\mu . \quad (28)$$

Next, we use Eq. 16 to represent $F_{1/2}$,

$$F_{1/2} = -\frac{2}{3\sigma_{n,1}\Delta x_1} (\phi_1 - \phi_{1/2}) , \quad (29)$$

where we have evaluated the face-averaged opacity with the cell-averaged value, i.e.

$$\sigma_{n,1/2}^+ = \sigma_{n,1} . \quad (30)$$

Substituting Eq. 28 into Eq. 29, an expression for the flux at the boundary of the DDMC region is

$$F_{1/2} = -\frac{2}{3\sigma_{n,1}\Delta x_1 + 6\lambda} \left(\phi_1 - 2 \int_0^1 W(\mu) I_b(X_L, \mu, t) d\mu \right) . \quad (31)$$

Using Eq. 31 in Eq. 24, the cell-centered equation for cell 1 is

$$\begin{aligned} \frac{1}{c} \frac{d}{dx} \phi_1 + (\sigma_{L,1} + \sigma_{R,1} + f_{n,1} \sigma_{n,1}) \phi_1 \\ = f_{n,1} \sigma_{n,1} a c T_{n,1}^4 + \frac{1}{\Delta x_1} \left(\sigma_{L,2} \phi_2 \Delta x_2 + \int_0^1 P(\mu) \mu I_b(X_L, \mu, t) d\mu \right) . \end{aligned} \quad (32)$$

In Eq. 32, the left-leakage opacity for cell 1 is given by

$$\sigma_{L,1} = \frac{1}{\Delta x_1} \frac{2}{3\sigma_{n,1}\Delta x_1 + 6\lambda} , \quad (33)$$

instead of Eq. 20, and $P(\mu)$ is defined as

$$P(\mu) = \frac{4}{3\sigma_{n,1}\Delta x_1 + 6\lambda} \left(1 + \frac{3}{2}\mu \right) . \quad (34)$$

Eq. 32 has a Monte Carlo interpretation similar to that of Eq. 19. The only difference on the left side is the expression for the left-leakage opacity. On the right side there is now a source due to Monte Carlo particles incident on the boundary of the DDMC region. We note that the rate at which radiation energy is incident on the DDMC region boundary for a given direction μ is μI_B . Then, $P(\mu)$ has the interpretation of being the probability that an incident Monte Carlo particle will be converted into a DDMC particle. This interface methodology is somewhat similar to the treatment developed by Brockway [18], except our technique is based on the asymptotic diffusion-limit boundary condition, whereas Brockway's is developed from the Marshak boundary condition.

We implement the conversion of Monte Carlo particles into DDMC particles in two separate ways. First, if the DDMC region is away from the problem boundary (e.g. $X_L \neq 0$), we sample based on Eq. 34 to determine if the incident Monte Carlo particle is converted. If the particle is converted, it begins transporting via DDMC in cell 1. Otherwise, the particle is returned isotropically to the optically thin region. DDMC particles that undergo left-leakage reactions in cell 1 are also placed isotropically on the boundary of the DDMC region. Although this is not the correct asymptotic albedo condition, it can be shown to be a good approximation [19].

If the DDMC region is on the boundary of the system (e.g. $X_L = 0$), then the incident Monte Carlo particles are actually source particles due to a prescribed surface source. In this case, we split the particles according to Eq. 34. The converted portion of the particle begins transporting via DDMC in cell 1, while the unconverted portion is tallied as escaping energy. DDMC particles that experience left-leakage reactions in cell 1 are also treated as escaping energy.

There are two difficulties when evaluating the conversion probability, Eq. 34. First, the conversion probability, along with the left-leakage opacity given by Eq. 33, vanishes as the opacity becomes large. Thus, no radiation can pass through the DDMC region boundary if the first cell is too optically thick. We correct this by adjusting the conversion probability and leakage opacity to ensure the correct flux is maintained at the boundary. For brevity we do not repeat this

analysis here, although documentation is available [20]. In addition, Eq. 34 must have a valid probabilistic interpretation, i.e.

$$0 \leq P(\mu) \leq 1 \quad . \quad (35)$$

In our DDMC method, we require that spatial cells are large enough such that Eq. 35 is always satisfied.

3.3. Estimation of Momentum Deposition

As was discussed earlier, coupled radiation-hydrodynamics calculations require an estimate of not only the radiation energy deposition in the material, but also the radiation momentum deposition. The estimation of energy deposition in DDMC is the same as in standard Monte Carlo; when a particle is absorbed its energy is allocated to the material. The specific momentum deposition is given by Eq. 7,

$$p(x,t) = \frac{\sigma}{c} \int_{-1}^1 \mu I(x,\mu,t) d\mu \quad , \quad (36)$$

and is straightforward to estimate in a standard Monte Carlo simulation. However, the estimation of momentum deposition in DDMC is difficult, since there is no angular information available to evaluate Eq. 36.

Instead, we use Eq. 10 to write Eq. 36 as a function of the radiative flux at a surface. For example, at $x = x_{j+1/2}$, we have

$$p_{j+1/2} = \frac{\sigma_{n,j+1/2}}{c} F_{j+1/2} \quad , \quad (37)$$

where we have employed an appropriate face-averaged value of the opacity. Then, for each cell we average the two cell-edge values of the momentum deposition in order to estimate the cell-averaged value:

$$P_j = \frac{1}{2c} \left(\sigma_{n,j-1/2}^+ F_{j-1/2} + \sigma_{n,j+1/2}^- F_{j+1/2} \right) \quad . \quad (38)$$

Note that we have evaluated Eq. 37 using the same face-averaged opacities used to calculate the leakage opacities (Eqs. 20, 21, and 33).

The flux in Eq. 38 can be calculated easily during a DDMC simulation. For instance, Eq. 18 can be expressed using Eqs. 20 and 21 as

$$F_{j+1/2} = \sigma_{R,j} \phi_j \Delta x_j - \sigma_{L,j+1} \phi_{j+1} \Delta x_{j+1} \quad . \quad (39)$$

Eq. 39 has interpretation of the rate at which particles undergo right-leakage reactions in cell j , minus the rate at which particles undergo left-leakage reactions in cell $j+1$. Similarly, Eq. 31 can be written using Eqs. 33 and 34 as

$$F_{1/2} = \int_0^1 P(\mu) \mu I_b(X_L, \mu, t) d\mu - \sigma_{L,1} \phi_1 \Delta x_1 \quad , \quad (40)$$

which can be interpreted as the rate at which Monte Carlo particles incident on the DDMC region boundary are converted into DDMC particles, minus the rate at which DDMC particles undergo left-leakage reactions in cell 1. Eqs. 39 and 40 can be used to evaluate Eq. 38 for each spatial cell in the problem.

Table I. Infinite Medium Timing Results

σ_0 (keV ³ /cm)	Monte Carlo Time (s)	DDMC Time (s)	Speedup
100	670	197	3.4
500	2.70E3	47	57
1000	5.25E3	27	190
5000	2.56E4	12	2100
10000	5.11E4	10	5100

4. NUMERICAL RESULTS

To demonstrate the accuracy and improved efficiency of our new DDMC method, we consider a series of radiative transfer problems simulated with IMC using both DDMC and standard Monte Carlo. In these problems we measure energy in gigajoules (gJ), time in nanoseconds (ns), and temperature in kiloelectron-volts (keV). In addition, unless otherwise stated, the material has a temperature-independent heat capacity of $C_v = 0.1$ gJ/cm³/keV, and an opacity inversely proportional to the cube of the material temperature,

$$\sigma = \frac{\sigma_0}{T^3} . \quad (41)$$

In the following simulations we use several values of σ_0 to test our improved DDMC method under various conditions.

4.1. Infinite Medium Problems

In the first set of problems, we examine a 1.0 cm thick slab with reflective boundary conditions. The matter and radiation are initially in equilibrium at 1 keV, and should remain in equilibrium indefinitely. We use a cell size of 0.1 cm, a time-step size of 0.1 ns, and 10,000 particles per time step. For each value of σ_0 we ran the simulation for an elapsed time of 10 ns using each of DDMC and standard Monte Carlo over the entire problem domain.

Every simulation, both standard Monte Carlo and DDMC, retained the correct equilibrium solution. The timing results of these simulations are give in Table I. Here, we have defined speedup as the computer time required by standard Monte Carlo divided by that required by DDMC. From these results we see that DDMC always increases the efficiency of the IMC calculation, from a factor of about 3 to over 5000. As expected, DDMC becomes more efficient, relative to standard Monte Carlo, as the opacity becomes larger.

4.2. Thermal Waves

The next set of problems consist of thermal waves driven by a surface source at 1 keV incident on the left boundary of the system. The material and radiation are initially in equilibrium at 0.001 eV. In these simulations the cell size is 0.005 cm, the time-step size is 0.01 ns, and we use

Table II. Isotropic Surface Source Timing Results

σ_0 (keV ³ /cm)	Monte Carlo Time (s)	DDMC Time (s)	Speedup
1000	5.40E4	1.09E3	49.5
5000	2.05E5	8.06E2	254
10000	3.59E5	7.82E2	459

Table III. Normal Surface Source Timing Results

σ_0 (keV ³ /cm)	Monte Carlo Time (s)	DDMC Time (s)	Speedup
1000	5.12E4	1.15E3	44.5
5000	1.99E5	7.89E2	252
10000	3.56E5	7.46E2	477

100,000 particles per time step. Again, for each value of σ_0 , the IMC calculation was performed using standard Monte Carlo or DDMC throughout the entire problem. Each simulation was run out to an elapsed time of 10 ns.

We first consider a thermal wave where the surface source is isotropic. The timing results from these simulations are presented in Table II. From this table, we see that DDMC improves the efficiency of the IMC calculation, with an increasing improvement as the opacity increases. For these problems the speedup ranged from about 40 to over 400.

We also plot the material temperature and momentum deposition at 10 ns for $\sigma_0 = 1000$ keV³/cm in Figures 1 and 2, respectively. These plots are characteristic of the results for other values of σ_0 . From Figure 1, the DDMC temperature agrees well with the standard Monte Carlo solution. Also, as seen in Figure 2, the momentum deposition results tend to match, especially near the wave front. However, both the DDMC and standard Monte Carlo momentum deposition estimates suffer severe statistical noise. This large amount of statistical error is characteristic of momentum deposition calculations.

In addition to an isotropic surface source, we also examine thermal waves driven by a normally incident surface source. This anisotropic incident intensity will induce a boundary layer and test the effectiveness of our improved interface method. The timing results for these simulations are give in Table III. Again, DDMC is more efficient than standard Monte Carlo, with a greater efficiency gain as the opacity increases.

The material temperature and momentum deposition at 10 ns for $\sigma_0 = 1000$ keV³/cm are plotted in Figures 3 and 4, respectively. As with the isotropic surface source problems, these plots are characteristic of the results for other values of σ_0 . From these figures we see that the DDMC solution matches the Monte Carlo results quite well. Again, both estimates of momentum deposition suffer from high statistical error. We also note that the temperature is slightly higher

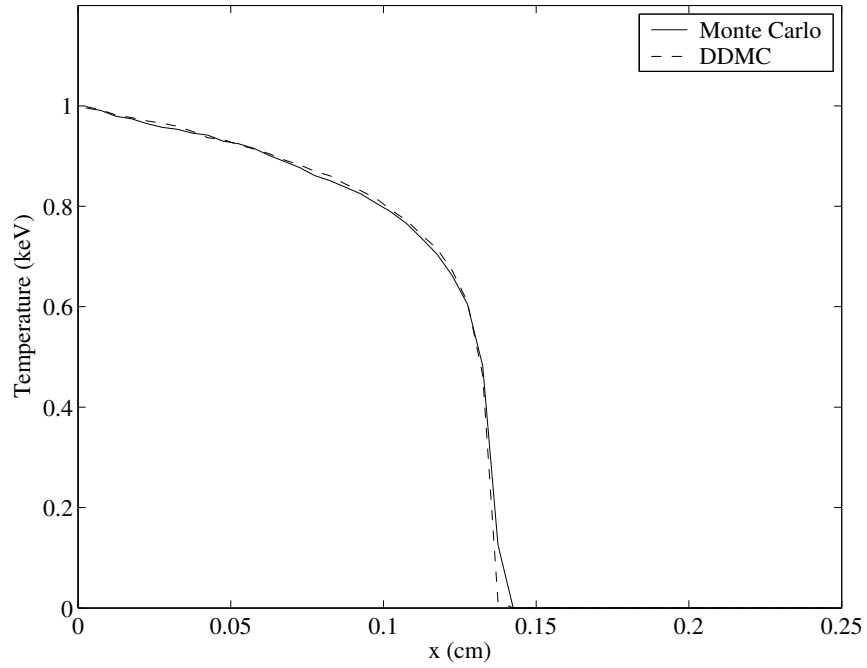


Figure 1. Isotropic Surface Source Material Temperature, $\sigma_0 = 1000 \text{ keV}^3/\text{cm}$

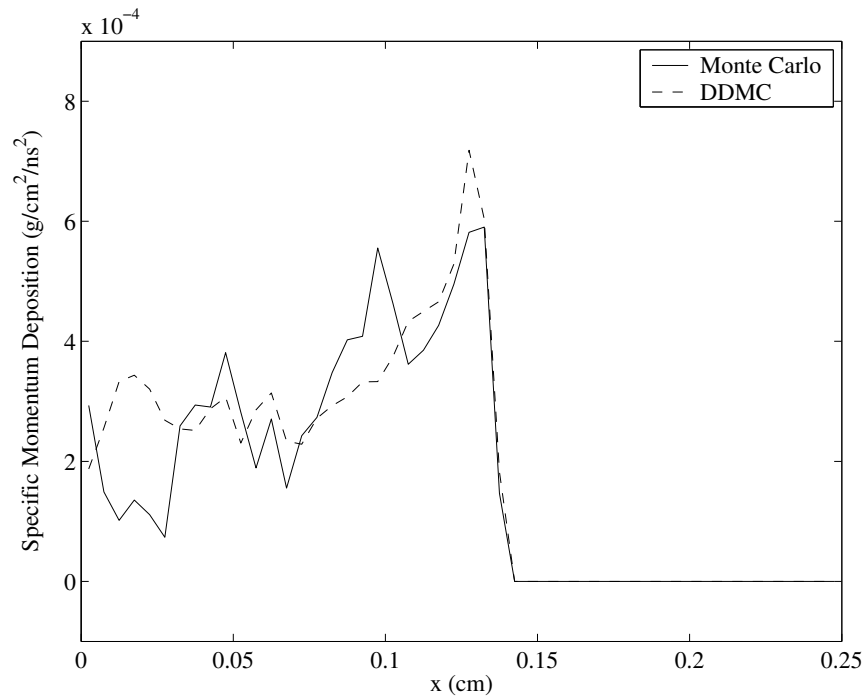


Figure 2. Isotropic Surface Source Momentum Deposition, $\sigma_0 = 1000 \text{ keV}^3/\text{cm}$

and the wave has progressed slightly farther in Figure 3 than in Figure 1. If we had employed a Marshak boundary condition as opposed to the asymptotic diffusion-limit boundary condition to develop our interface method, the material temperature calculated by DDMC would be identical in Figures 3 and 1, which is incorrect for a normally incident intensity.

4.3. Hybrid Problems

We now consider two problems with both optically thick and optically thin regions. We model the optically thick region with an opacity given by Eq. 41 with $\sigma_0 = 1000 \text{ keV}^3/\text{cm}$. The optically thin region has a temperature-independent opacity of 1 cm^{-1} . The material and radiation are initially in equilibrium at 0.001 eV, and the left boundary has a surface source at 1 keV. In these simulations, the cell thickness is 0.005 cm in the optically thick region, 0.02 cm in the optically thin region, the time-step size is 0.01 ns, and we use 100,000 particles per time step.

To solve these problems we employ standard Monte Carlo in the optically thin region, and either standard Monte Carlo or DDMC in the optically thick region. The pure Monte Carlo calculation serves as our benchmark solution, while the hybrid Monte Carlo-DDMC simulation will test the accuracy and efficiency of DDMC.

In the first problem the surface source is isotropic, and the left-most region consists of 0.1 cm of optically thick material followed by a 0.4 cm optically thin region. The right boundary is reflective such that the problem will eventually reach equilibrium at 1 keV. Each simulation was run to 150 ns.

The material temperature at 10, 20, and 150 ns is plotted in Figure 5. From this figure we see that the DDMC results agree fairly well with the standard Monte Carlo solution, and both methods produced the correct equilibrium solution. In Figure 6 we plot the specific momentum deposition at 10 ns. From this plot it appears that the DDMC simulation overestimates the peak momentum deposition with respect to standard Monte Carlo. This error is most likely caused by DDMC momentum deposition being estimated at cell edges, while standard Monte Carlo momentum deposition is estimated as a cell average. The standard Monte Carlo simulation required 120 hours of computer time, while DDMC used 5.6 hours, for a speedup of over 20.

In the second problem the surface source is normally incident, and the left-most region is 1 cm of optically thin material followed by 0.5 cm of optically thick material. Each simulation was run for an elapsed time of 50 ns. Since the optically thin region is a mean-free path thick, the intensity reaching the optically thick region is fairly anisotropic. Thus, using our improved interface method is important.

The resulting material temperature at 0.5, 1.5, and 50 ns is plotted in Figure 7. Again, the DDMC results agree well with the standard Monte Carlo solution. In addition, we plot the specific momentum deposition at 0.5 ns in Figure 8. Most momentum deposition occurred only in a few cells. However, the DDMC estimate was within 1.6% of the standard Monte Carlo solution at the peak value. For this problem standard Monte Carlo took 28.6 hours, while DDMC required 2.2 hours, for a speedup of about 13.

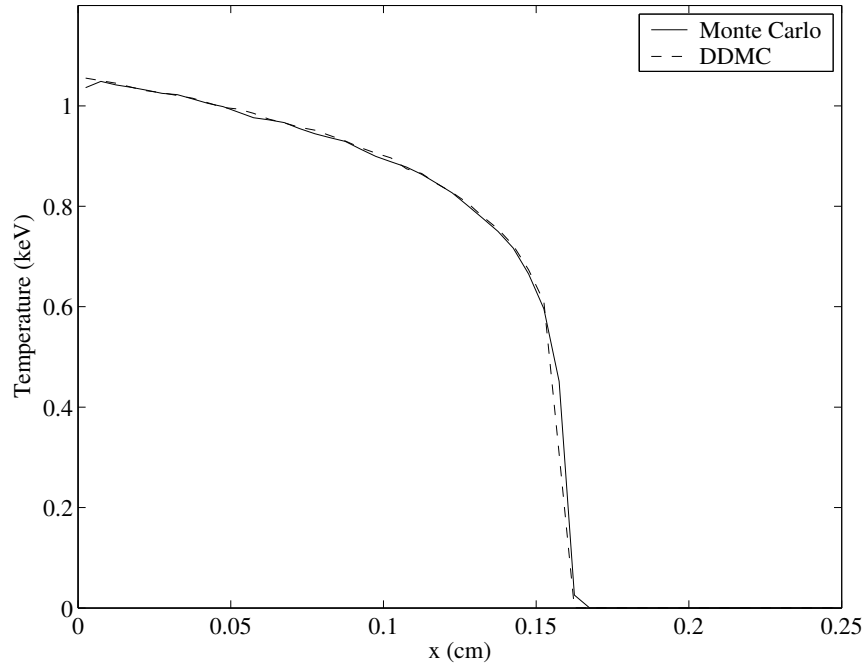


Figure 3. Normal Surface Source Material Temperature, $\sigma_0 = 1000 \text{ keV}^3/\text{cm}$

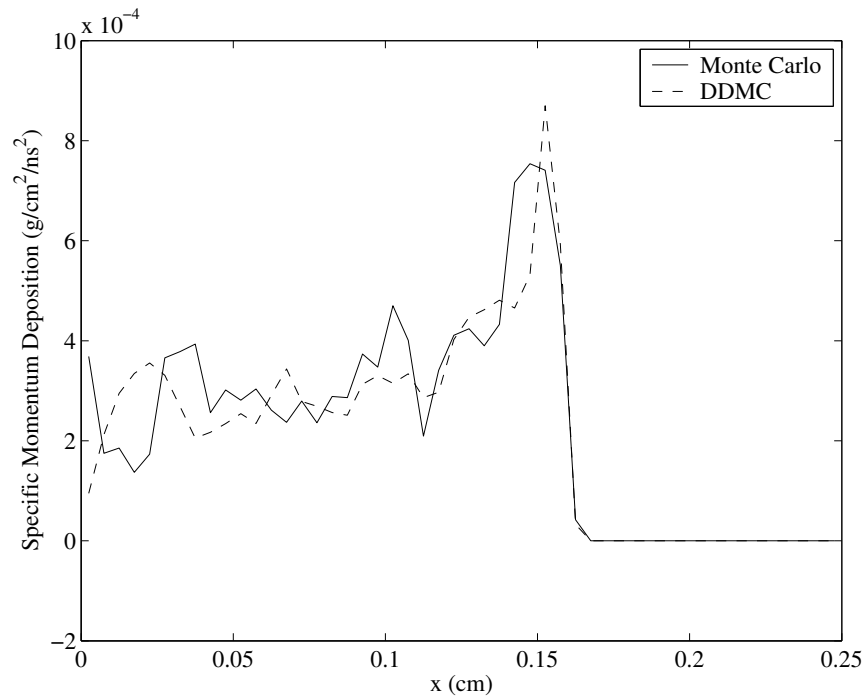


Figure 4. Normal Surface Source Momentum Deposition, $\sigma_0 = 1000 \text{ keV}^3/\text{cm}$

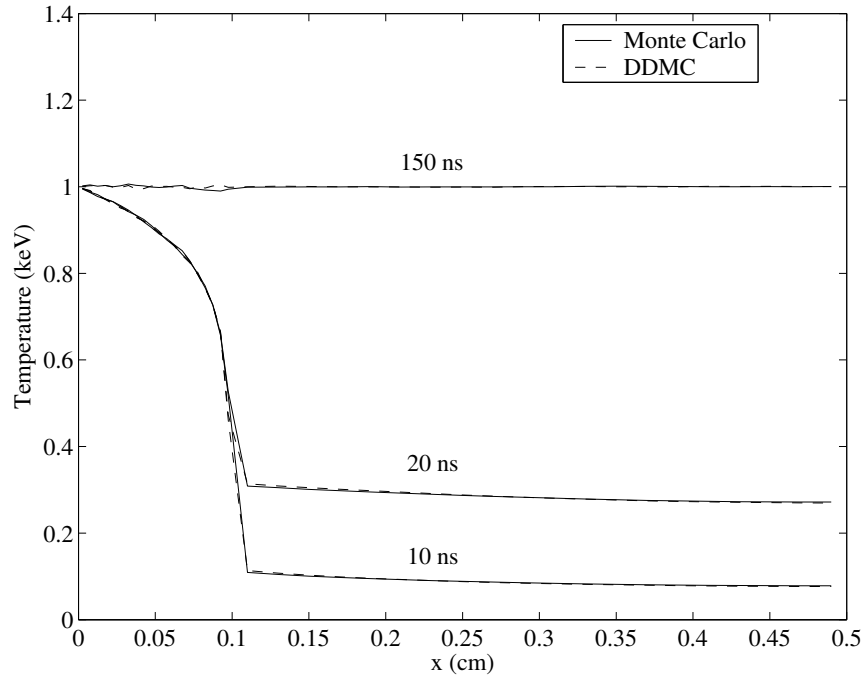


Figure 5. First Hybrid Problem Material Temperature

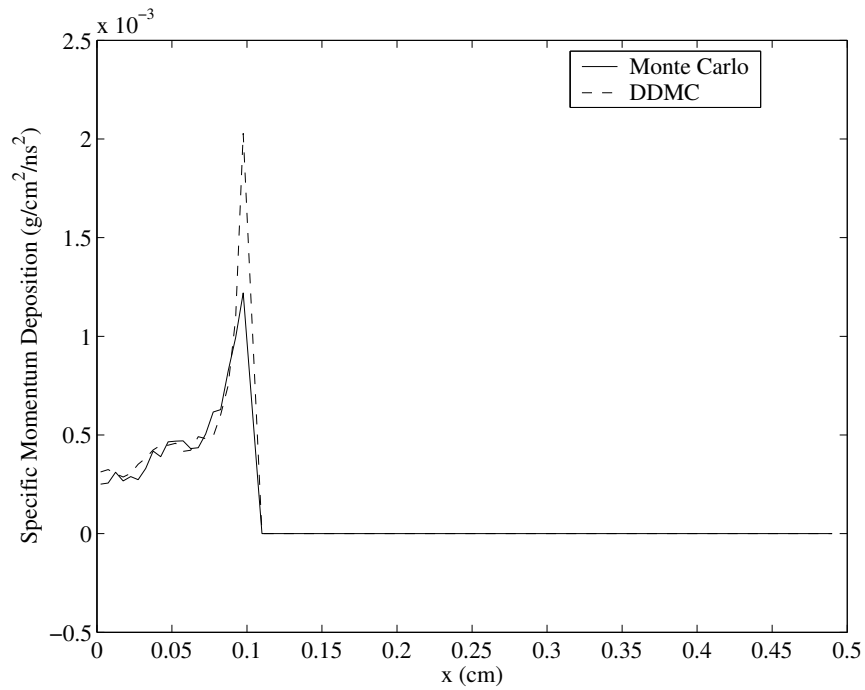


Figure 6. First Hybrid Problem Momentum Deposition

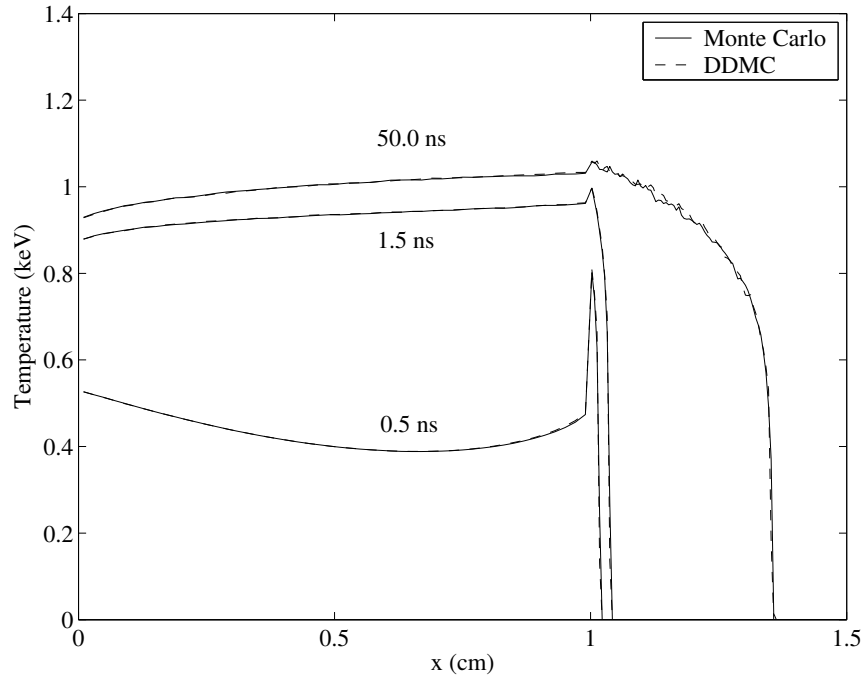


Figure 7. Second Hybrid Problem Material Temperature

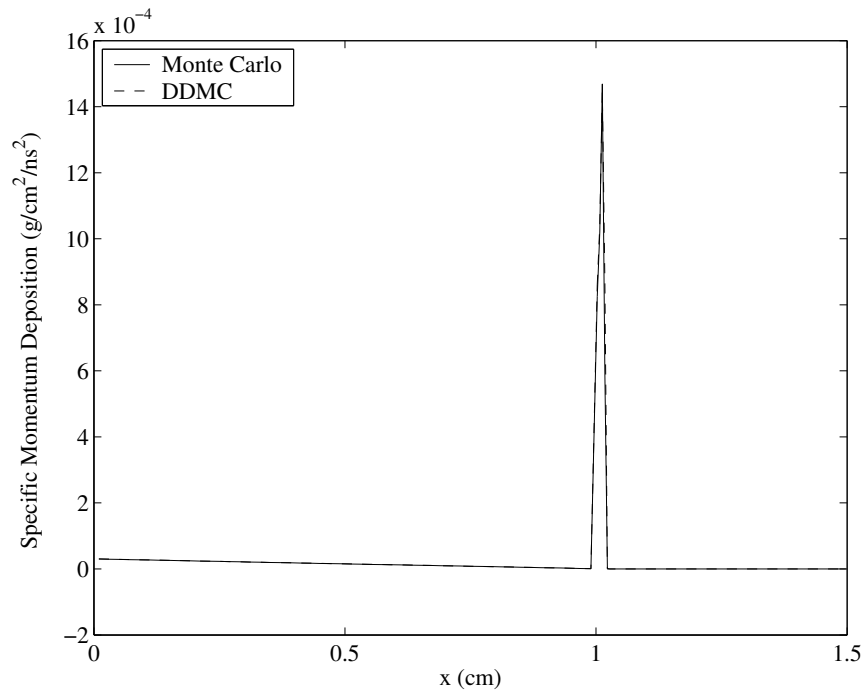


Figure 8. Second Hybrid Problem Momentum Deposition

5. CONCLUSIONS

We have extended previously developed DDMC methods in several ways that improve the accuracy and utility of DDMC for grey IMC simulations. First, we base our DDMC method on a temporally continuous diffusion equation. This lack of temporal discretization results in a theoretically more accurate DDMC calculation, and no ambiguity regarding what time to assign to DDMC particles that are converted to Monte Carlo particles. Also, we employ a technique for interfacing standard Monte Carlo and DDMC based on the asymptotic diffusion-limit boundary condition. This technique can produce accurate results regardless of the angular distribution of incident Monte Carlo particles. Finally, we develop a method for estimating momentum deposition in DDMC simulations. This momentum deposition estimate is required to correctly calculate fluid motion in coupled radiation-hydrodynamics problems.

With a set of numerical calculations, we have demonstrated the accuracy and improved efficiency of our new DDMC method as compared to standard Monte Carlo. However, our estimates of momentum deposition, both using DDMC and standard Monte Carlo, exhibited a large amount of statistical error. The reduction of this statistical noise is the subject of current research.

We also note that, in our numerical simulations, the region in which DDMC was employed was always determined *a priori*. In order for DDMC to be used in practical calculations, a technique for automatically determining when and where to employ DDMC must be developed. In addition, the one-dimensional, grey DDMC method presented here must be extended to multi-dimensional, frequency-dependent problems. These issues remain for future work.

ACKNOWLEDGMENTS

We would like to thank David Carrington for suggesting the use of face-averaged opacities when estimating momentum deposition. This work was performed under U.S. Government contract W-7405-ENG-36 for Los Alamos National Laboratory, which is operated by the University of California for the U.S. Department of Energy.

REFERENCES

1. J. A. Fleck, Jr., J. D. Cummings, "An Implicit Monte Carlo Scheme for Calculating Time and Frequency Dependent Nonlinear Radiation Transport," *J. Comp. Phys.*, **8**, p. 313 (1971).
2. E. W. Larsen, B. Mercier, "Analysis of a Monte Carlo Method for Nonlinear Radiative Transfer," *J. Comp. Phys.*, **71**, p. 50 (1987).
3. W. R. Martin, F. B. Brown, "Error Modes in Implicit Monte Carlo," *Trans. Am. Nucl. Soc.*, **85**, p. 329 (2002).
4. J. A. Fleck, Jr., E. H. Canfield, "A Random Walk Procedure for Improving the Computational Efficiency of the Implicit Monte Carlo Method for Nonlinear Radiation Transport," *J. Comp. Phys.*, **54**, p. 508 (1984).
5. J. Giorla, R. Sentis, "A Random Walk Method for Solving Radiative Transfer Equations," *J. Comp. Phys.*, **70**, p. 145 (1987).
6. T. J. Urbatsch, J. E. Morel, J. Gulick, "Monte Carlo Solution of Spatially-Discrete Transport Equations, Part II: Diffusion and Transport-Diffusion," *Proc. Int. Conf. Mathematics and*

- Computation, Reactor Physics, and Environmental Analysis in Nuclear Applications*, Madrid, Spain, September 27–30, 1999, Vol. 1, p. 262.
7. T. M. Evans, T. J. Urbatsch, H. Lichtenstein, “1-D Equilibrium Discrete Diffusion Monte Carlo,” *Proc. MC2000 — International Conference*, Lisbon, Portugal, July, 2000.
 8. N. A. Gentile, “Implicit Monte Carlo Diffusion — An Acceleration Method for Monte Carlo Time-Dependent Radiative Transfer Simulations,” *J. Comp. Phys.*, **172**, p. 543 (2001).
 9. E. W. Larsen, G. C. Pomraning, V. C. Badham, “Asymptotic Analysis of Radiative Transfer Problems,” *J. Quant. Spectrosc. Radiat. Transfer*, **29**, p. 285 (1983).
 10. J. D. Densmore, “An Improved Method for Treating Monte Carlo-Diffusion Interfaces,” *Trans. Am. Nucl. Soc.*, **91**, p. 139 (2004).
 11. G. J. Habetler, B. J. Matkowsky, “Uniform Asymptotic Expansions in Transport Theory with Small Mean Free Paths, and the Diffusion Approximation,” *J. Math. Phys.*, **16**, p. 846 (1975).
 12. G. I. Bell, S. Glasstone, *Nuclear Reactor Theory*, Krieger Publishing, Malabar, Florida (1985).
 13. D. Mihalas, B. Weibel-Mihalas, *Foundations of Radiation Hydrodynamics*, Dover Publications, Mineola, New York (1999).
 14. J. I. Castor, *Radiation Hydrodynamics*, Cambridge University Press, Cambridge, United Kingdom (2004).
 15. G. C. Pomraning, *The Equations of Radiation Hydrodynamics*, Pergamon Press, Oxford, United Kingdom (1973).
 16. E. E. Lewis, W. F. Miller, Jr., *Computational Methods of Neutron Transport*, American Nuclear Society, La Grange Park, Illinois (1993).
 17. R. H. Szilard, G. C. Pomraning, “Numerical Transport and Diffusion Methods in Radiative Transfer,” *Nucl. Sci. Eng.*, **112**, p. 256 (1992).
 18. G. C. Pomraning, G. M. Foglesong, “Transport-Diffusion Interfaces in Radiative Transfer,” *J. Comp. Phys.*, **32**, p. 420 (1979).
 19. C. J. Gesh, M. L. Adams, “Finite Element Solutions of Second-Order Forms of the Transport Equation at the Interface between Diffusive and Non-Diffusive Regions,” *Proc. Int. Mtg. Mathematical Methods for Nuclear Applications*, Salt Lake City, Utah, September 9–13, 2001.
 20. J. D. Densmore, D. B. Carrington, “Emissivity of Discretized Diffusion Problems,” Tech. Rep. LA–UR–05–3249, Los Alamos National Laboratory (2005).